

Numerical simulations of sheet-metal forming

L. Taylor^{a,*}, J. Cao^a, A.P. Karafillis^a, M.C. Boyce^b

^a*Hibbit, Karlsson & Sorensen, Inc., Pawtucket, RI 02860, USA*

^b*Massachusetts Institute of Technology, Cambridge, MA 02139, USA*

Industrial Summary

The objective of this paper is to discuss the numerical solution of sheet-metal forming applications using the ABAQUS general purpose implicit and explicit finite-element modules. The three conference benchmark problems of NUMIFORM'93 are used as examples in the paper. The analyses were performed using combinations of the implicit and explicit versions of ABAQUS. The numerical-modeling techniques used in these analyses are discussed. The effectiveness and suitability of the implicit and explicit finite-element procedures for each of the benchmark problems are discussed.

1. Introduction

In the past decade, there has been a tremendous advance in the usage of finite-element simulations for sheet-forming processes. For a variety of recent applications see, for instance, the proceedings of NUMIFORM'89 [1], NUMIFORM'91, International Conference on Developments in Forming Technology [2], or FE-Simulation of 3-D Sheet Metal forming Processes in Automotive Industry [3]. These advances can, for the most part, be attributed to two factors: (i) the exponential increase in the raw cpu speed of the hardware available for the analysis; and (ii) the maturing of the finite-element software available for the analysis. In particular, the emergence of the explicit dynamics finite-element procedure in conjunction with modern vector/parallel hardware has led to the development of effective general-purpose software packages for this type of analysis. However, the traditional implicit statics finite-element program still plays a major role in the analysis of this class of problems. In particular, spring-back prediction is more suited to a statics algorithm, as will be discussed below. A further advantage of the implicit general-purpose finite-element program is that it offers additional procedures such as eigenvalue extraction and heat-transfer calculations.

* Corresponding author.

The explicit dynamics algorithm has several key advantages over a conventional implicit statics algorithm for sheet-metal forming problems. First, there is no direct, banded, linear equation solver. Consequently, the computational cost of a solution does not grow quadratically with the problem size. In general, computational cost scales linearly with problem size in the explicit dynamics procedure. Second, large deformation, sliding, three-dimensional contact constraints are relatively easy to implement in an explicit procedure. The kinematic contact constraints can be enforced explicitly as a predictor/corrector algorithm and, since there is no equation solver, changing contact conditions do not require bandwidth optimization considerations. The major disadvantage of the explicit dynamics procedure is that it is a dynamics procedure. Generally, this requires that some sort of artificial time scale must be introduced into the analysis to achieve an economical solution. Typically, the dynamic sheet-metal forming analysis is performed at punch velocities on the order of 5–20 m/s, with the assumption that this approximates the quasistatic solutions. Nagtegaal and Taylor [4] and Rebelo, et al. [5] contain more detailed discussions of the implicit versus explicit finite-element techniques.

In this paper is presented numerical solutions to the three benchmark problems for NUMISHEET'93 comparing use of the two solution procedures as well as use of different yield criteria. The analyses are all performed using either ABAQUS/Standard [6] or ABAQUS/Explicit [7].

2. Two-dimensional bending problems

For the 2-D bending benchmark problems, a sheet of metal is clamped by a constant blank holding force and then subjected to bending (Fig. 1). The final shape upon

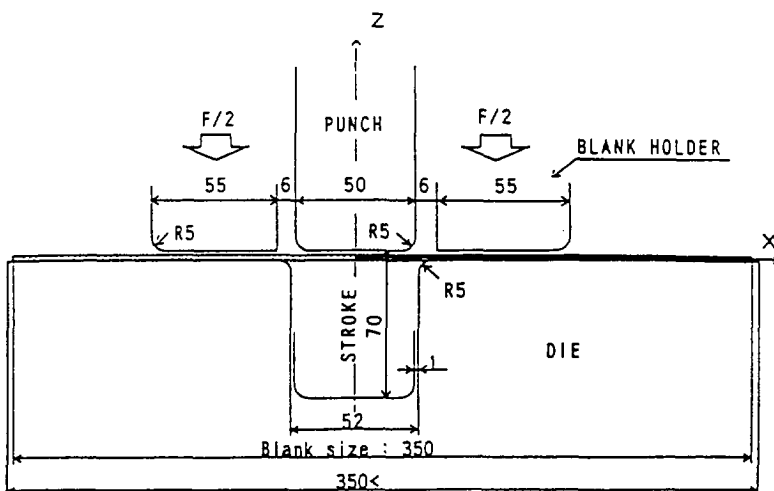


Fig. 1. Schematic of a 2-D bending problem (Numisheet'93 handout) (dimensions:mm).

unloading is sought. The spring-back in this problem is expected to be very large and the elastic–plastic behavior of the material and the bending of the sheet must be modeled accurately.

Each material is modeled as elastic–plastic where the elasticity is taken to be isotropic and the plasticity is modeled as anisotropic using the Hill quadratic anisotropic yield criterion. The material constants were obtained using the R -ratios and the yield strength in the rolling direction of each material. The material properties (elastic constants, yield strength, R -ratios) and yield criterion constants for each material are listed in Table 1, where subscript 1 corresponds to the rolling direction, 2 to the direction perpendicular to 1 in the blank plane, and 3 to the direction through the thickness, and where $\tau_0 = \sigma_0/\sqrt{3}$.

Table 2 provides a summary of the simulations conducted where effects of element formulation, material, and binder force are examined. Due to the symmetry of the geometry, loading and boundary conditions, only one-half of the blank was modeled. Since the blank depth/thickness ratios was 35.0 mm/0.78 mm, the bending was modeled as a plane-strain problem. For the cases using the implicit procedure, the blank was modeled with either: (i) 8-node plane strain reduced integration elements using 2 elements through the thickness and 150 elements along the length; or

Table 1
Material properties and yield-criterion constants

Material	E (GPa)	σ_0 (MPa)	r_0	r_{45}	r_{90}	σ_{11}/σ_0	σ_{22}/σ_0	σ_{33}/σ_0	σ_{12}/σ_0
Mild steel ^a	206.0	167.0	1.79	1.51	2.27	1.0	1.0402	1.24897	1.07895
High tensile steel ^a	206.0	296.5	1.73	1.34	2.24	1.0	1.0445	1.2411	1.12148
Aluminum ^a	71.0	137.0	0.71	0.58	0.70	1.0	0.9958	0.9214	1.08585
Aluminum ^b	71.0	137.0	0.71	0.58	0.70	1.0	0.988	0.945	0.977

^a Material properties for the Hill quadratic anisotropic yield criteria.

^b Material properties for the Karafillis and Boyce [9] yield criteria.

Table 2
List of simulations of the 2-D bending problem

Case	Material	Force (KN)	Element type	No. of elements
1	Mild steel	19.6	Continuum CPE8R	150 × 2
2	Mild steel	19.6	Sheel S4RF	180 × 1 × 1
3	Aluminum	19.6	Continuum CPE8R	150 × 2
4	High tensile steel	19.6	Continuum CPE8R	150 × 2
5	Mild steel	2.45	Continuum CPE8R	150 × 2
6	Aluminum	2.45	Continuum CPE8R	150 × 2
7	High tensile steel	2.45	Continuum CPE8R	150 × 2

(ii) 4-node reduced integration shell elements with 180 elements along the length. In all cases, the punch, die and blankholder were modeled as rigid surfaces. The use of continuum vs. shell elements was examined using the implicit procedure with mild steel as the material and a blank-holding force of 19.6 kN (cases 1 and 2 of Table 2). The effect of the material was examined by comparing cases 1, 3 and 4. The effect of the binder force (19.6 kN vs. 2.45 kN) was also examined for each of the three materials. Excellent agreement was obtained between the two simulations where the plane strain and shell elements were used (cases 1 and 2); for brevity, the shell results are not shown in the figures which follow.

The effects of the material and the blank-holding force on the shape produced are shown in Fig. 2. All of these cases used the 8-node plane strain continuum elements and the implicit procedure. First, comparing the results of each material when the 19.6 kN blank-holding force was used, the dramatic effect is seen of the ratios of the yield stress to the elastic modulus on the spring-back. Much larger amounts of spring-back are observed in the aluminum and high tensile strength steel because of the larger elastic contribution to the deformation than in the case of the mild steel. The (initial) yield stress/modulus ratios are 1.93×10^{-3} , 1.31×10^{-3} and 0.81×10^{-3} for the aluminum, high tensile steel and mild steel, respectively. Note also that the greater is the magnitude of this ratio, then the greater is the effect of the blank-holding force on the spring-back, as shown also in Fig. 2.

Simulations of the 2-D bending problem were performed using ABAQUS/Explicit with a mesh of lower-order continuum elements with four elements through the thickness and 320 elements along the length. However, spring-back due to unloading is not yet complete due to inertial effects, as shown in Fig. 2. In the explicit dynamics analysis, the time period required for the spring-back is extremely long compared to

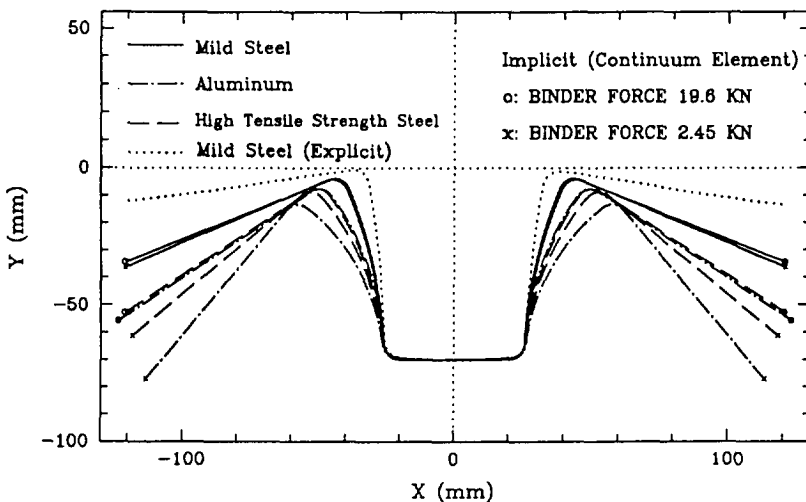


Fig. 2. Computed unloading shapes.

the stable time increment required for this procedure. During the forming operation, it is possible to artificially increase the speed of the process because the inertial effects are small and the analysis is essentially kinematically constrained. However, during the spring-back step, the blank responds inertially. Hence, it is seen that the response is one of free vibration in the lowest structural mode. The time period required for the structure to damp out to an equilibrium solution is simply too long to enable an economical solution to the spring-back to be obtained.

3. Forming of a square cup

In this problem, a square cup is punched out of sheet material. The geometry and dimensions are shown in Fig. 3. The primary quantities of interest are the strain distribution produced in the formed product. Due to the geometry of the shape and the anisotropy of the material, a one-quarter model of the cup can be analyzed. Since unloading (spring-back) is not considered in this problem, the use of the explicit solution procedure and shell elements will provide the most computationally efficient simulation. The size of the original square blank is 15 mm \times 15 mm. A 60 \times 60 mesh of 4-node reduced integration shell elements is used in the one-quarter model of the blank. The blank-holder, die and punch were modeled as rigid surfaces. Friction between the blank and the surfaces was modeled using Coulomb friction with a friction coefficient of 0.162. The average speed of the punch during the stamping

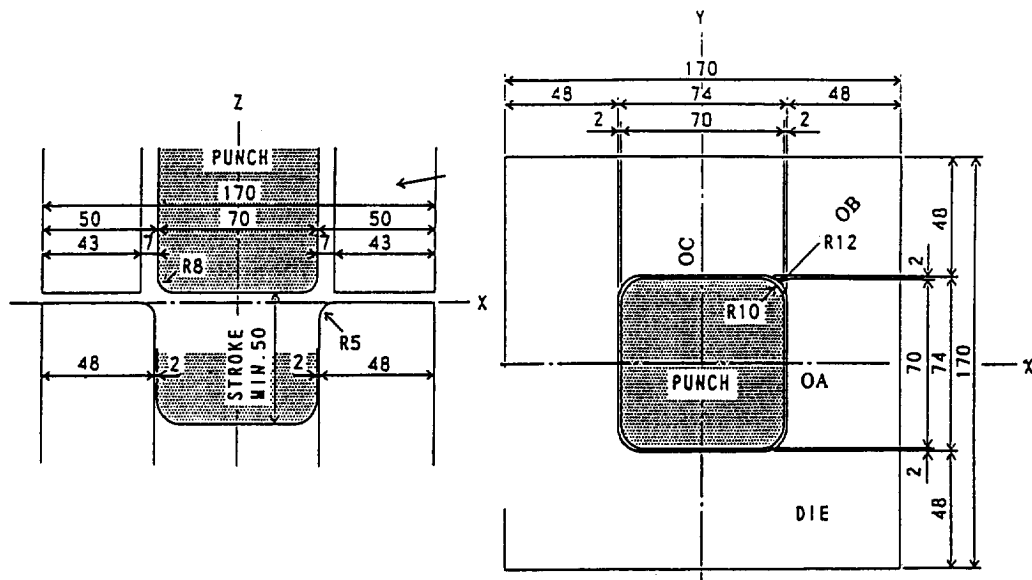


Fig. 3. Schematic of the square cup problem (Numisheet'93 handout).

procedure was 8 m/s for most cases. One case was run at 30 m/s to investigate sensitivity to this parameter. The blank-holding force for the one-quarter model is 4.9 kN (19.6 kN for the full cup).

Aluminum material was considered in this problem. Due to the predicted sensitivity of the plastic behavior of the aluminum to the yield criterion used [19], three yield criteria were considered in the simulations, the three criteria being: (i) the Mises isotropic yield criterion; (ii) the Hill quadratic anisotropic yield criterion; and (3) the non-quadratic anisotropic yield criterion of Karafillis and Boyce [10] which maps the anisotropy using a set of tensorial state variables. Isotropic hardening was considered in all three cases. The R -ratios were provided for three different directions and were used to obtain the anisotropic constants in both the Hill and the Karafillis and Boyce criteria. Material properties and derived model constants are listed in Table 1. The yield stress of the material showed negligible dependence of direction; the R -ratios in the 0° and 90° directions were nearly identical (0.71 vs. 0.70), but relatively large anisotropy was exhibited in the 45° direction (0.58). The planar yield surfaces obtained for the three yield criteria are shown in Fig. 4, illustrating the strong sensitivity of yield-surface shape (and thus the normal to the yield surface) on the criterion, which implies the dependency of material straining on the yield criterion.

The comparison of the through-thickness strain distributions obtained using the three yield criteria and the two different punch velocities at a punch travel of 40 mm are illustrated in Figs. 5 and 6, for the OA path and the OB path, respectively. By comparing the Hill and Mises criteria, a significant difference in the strain distributions is detected, which indicates a strong influence of the anisotropic behavior especially with regard to localized thinning. It is noted also that the K-B

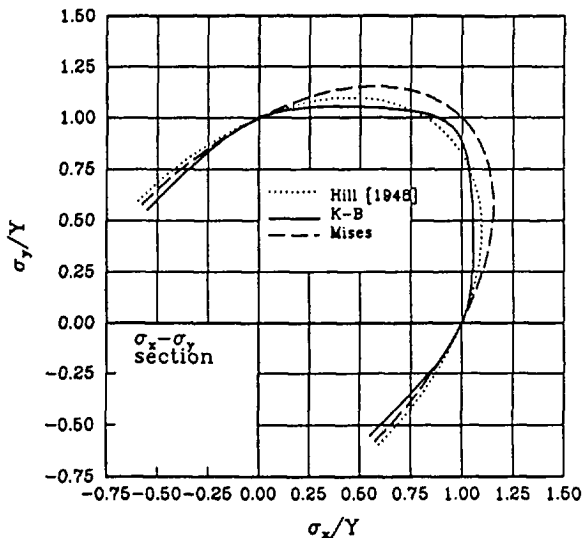


Fig. 4. Yield surface of the aluminum material.

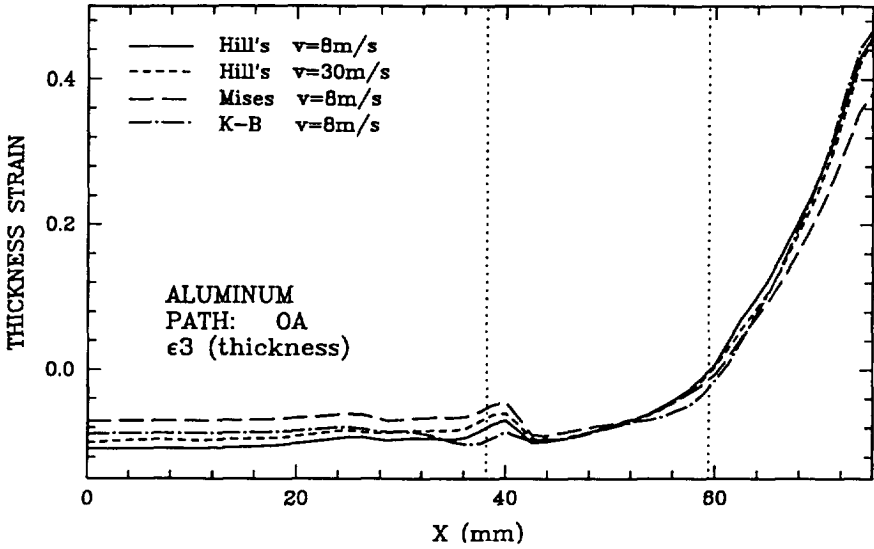


Fig. 5. Comparison of the through-thickness strain distribution using various yield criteria (line OA).

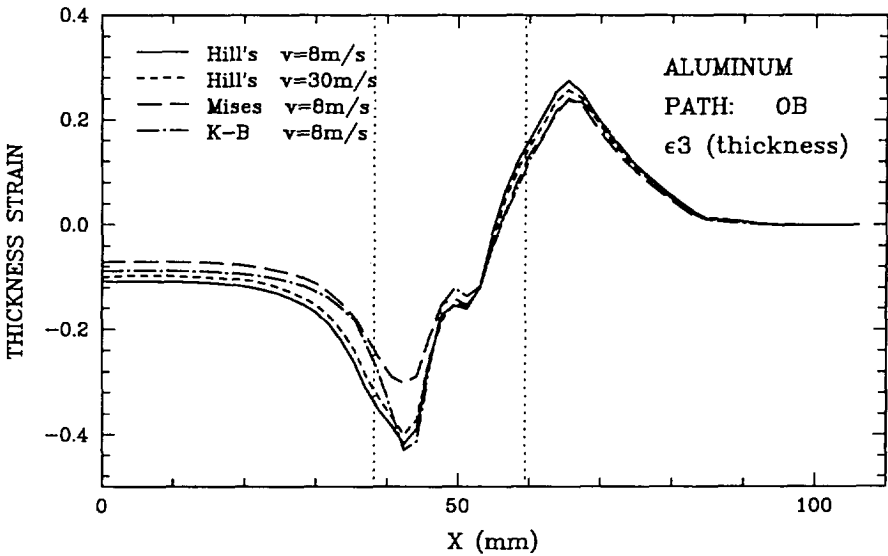


Fig. 6. Comparison of the through-thickness strain distribution using various yield criteria line OB).

non-quadratic yield criterion predicted more localized thinning than the other criteria, where it is noted that thinning is normally under-predicted in aluminum materials. Also, the higher punch-velocity simulation does not capture the strain localization as well as the slower run under otherwise identical conditions.

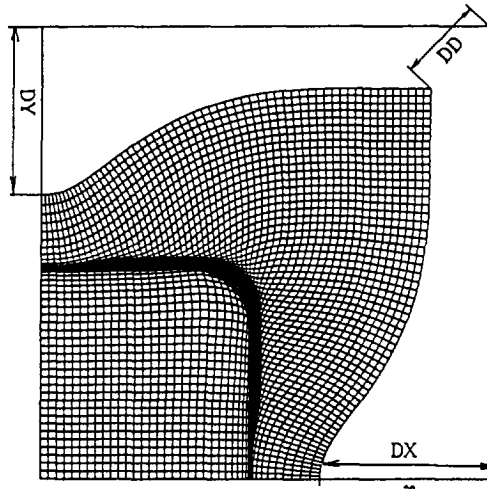


Fig. 7. Deformed shape of the square cup on the x - y plane.

Table 3

Comparison of the amount of draw-in obtained for various yield criteria

Yield criterion	DX (mm)	$DX/DX_i - 1$ (%)	DY (mm)	$DX/DX_i - 1$ (%)	DD (mm)	$DD/DD_i - 1$ (%)
Mises	28.365	0.	28.375	0.	14.911	0.
Hill	27.452	- 3.219	27.321	- 3.715	14.662	- 1.670
K-B	27.944	- 1.484	27.978	- 1.399	14.604	- 2.059

Fig. 7 shows the x - y projection of the deformed shape after 40 mm of punch travel, the amount of draw-in at different locations, DX , DY , and DD , being defined in the figure. Table 3 lists the amounts of draw-in in these three directions at a punch travel of 40 mm obtained from using the three yield criteria, where subscript i indicates the results from the Mises isotropic yield criterion. These results also show effects on the deformation from the relatively small amount of material anisotropy.

4. Front-fender simulation

The simulation of the front fender stamping was performed using ABAQUS/Explicit. The size of the model and the geometrically complex contact constraints dictate the use of an explicit-integration-procedure approach in the analysis. However, preliminary calculations were performed with ABAQUS/Standard to determine the material restraining forces provided by five different drawbead geometries. The small size of the drawbead geometries represents a challenge from the perspective of

modeling the blank. The drawbeads are on the order of 5 mm, and if their geometry is to be included in the mesh of the tools, would dictate a mesh size on the blank on the order of 1 mm. Such a small mesh would result in cpu time requirements that would not be practical.

Two dimensional plane-strain calculations were performed using ABAQUS/Standard for each of the drawbead geometries. Two layers of 8-node reduced integration continuum elements were used to describe the blank. The interaction between the blank and the rigid surface of the drawbeads was modeled using a penalty-based contact algorithm; also, frictional slip was modeled using a yield function in the slip-displacement space where a limited amount of elastic slip was allowed prior to plastic (irreversible) slip [10]. This method was found to be very effective when modeling drawbeads, see also Ref. [11]. Fig. 8 shows the calculated restraining force versus pull-out displacement for each of the five drawbead geometries. It is noted that the restraining forces were obtained with a penetration of the drawbeads which allowed a 1.4 mm clearance between the die and the binder. As shown in Ref. [11], even small variations of the clearance and the geometry of the drawbeads have a dramatic effect on the restraining force. Therefore, the reliability of the simulation results depends on the precision of the provided geometric data and clearance.

In the three-dimensional stamping simulation, the restraining forces were applied to the blank as a set of frictional forces between the blank and a set of nodes along the drawbead centerlines. A truss element was attached to each drawbead node, the truss

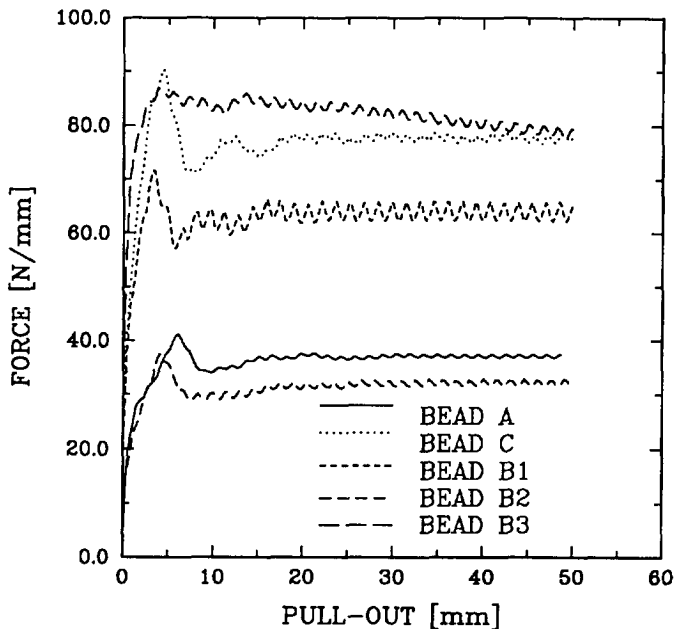


Fig. 8. Computed restraining forces for each of the 5 drawbead geometries.

elements being used in order to minimize vibrations and bouncing in the drawbead nodes by providing some dissipation through plasticity in the material of the truss elements. A unique local coordinate system was defined at each of the 1215 drawbead nodes (also to the second node of each truss element) in which the local 3 direction was normal to the tool, and the local 1 and 2 directions were tangential to the tool. The truss elements are all aligned with the local 3 direction. Zero displacement boundary conditions were applied in the local 1 and 2 directions at each drawbead node. The drawbead nodes have a degree of freedom in the local 3 direction, but they have a contact constraint that they may not penetrate the top of the blank. To the other end of the truss, a compressive concentrated load is applied along the axis of the truss (the local 3 direction) developing a normal force on the surface of the blank through the contact constraint. The coefficient of friction used was 0.3, and for each of the 5 drawbead geometries a normal force was chosen so that the tangential friction force on the surface of the blank matches the steady-state value found in Fig. 8. Fig. 9 shows the position of the drawbead nodes on the blank in the binder-closed position.

The blank was modeled with 3975 shell elements (75×53 mesh). The analysis was performed in a series of steps. In the first step, the binder was closed to place the blank in contact with the die. The next step was to develop the drawbead forces. The concentrated loads on each of the draw beads were ramped up during this step. The final step was to move the punch down to form the fender. Fig. 10 shows the deformed shape of the blank in its final position (1 mm up).

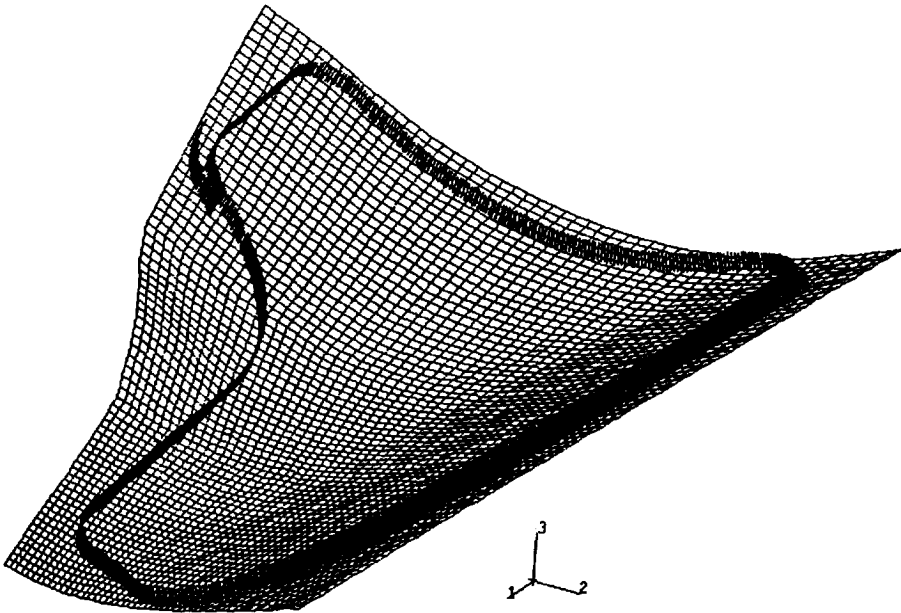


Fig. 9. Location of drawbead nodes on the blank in the binder-closed position.

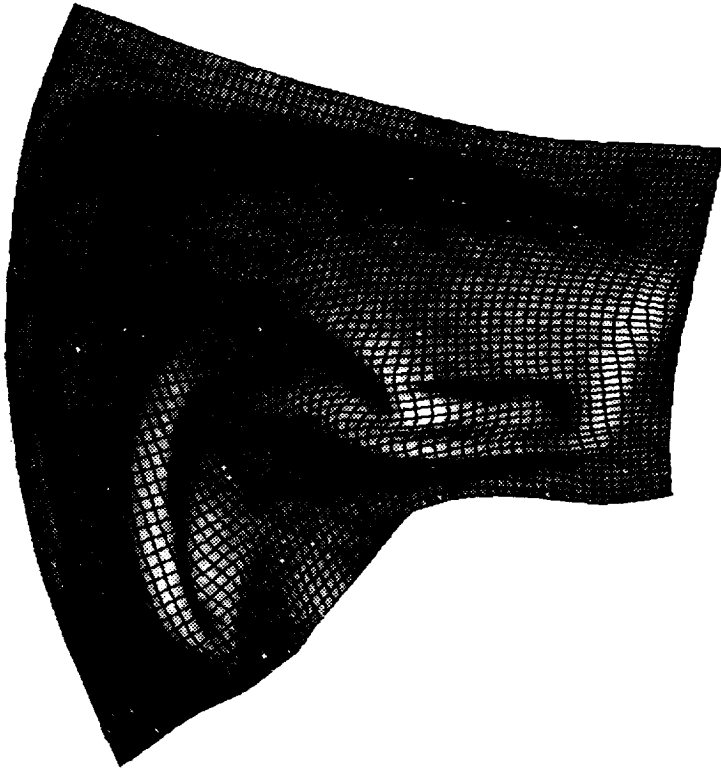


Fig. 10. The deformed shape of the blank in the final position (1 mm up).

5. Closure

The results of the analyses presented here indicate that complex three-dimensional sheet forming problems can be analyzed successfully utilizing both the implicit and explicit finite element technique for the portions of the problem for which they are best suited. In general, for the forming of large three-dimensional parts such as those found commonly in automotive stampings, the explicit dynamics procedure is the method of choice.

References

- [1] E.G. Thompson, R.D. Wood, O.L. Zeinkiewicz and A. Samuelsson (eds.), *Proc. Third Int. Conf. on Numerical Methods in Industrial Forming Processes*, Balkema, Rotterdam, 1989.
- [2] *Proc. Int. Conf. on Developments in Forming Technology*, *J. Mats. Proc. Tech.* 24 (1990).
- [3] J. Reissner et al. (Eds.), *Proc. FE-Simulation of 3-D Sheet Metal forming Processes in Automotive Industry*, VDI-Verlag, Dusseldorf, 1991.

- [4] J.C. Nagtegaal and L.M. Taylor, Comparison of implicit and explicit finite element methods for analysis of sheet forming processes, in: J. Reissner et al. (Eds.), *Proc. of the FE-Sim of 3-D Sheet Metal Form. Proc. in Automotive Ind. Conf.*, VDI Berichte 894, VDI-Verlag, Dusseldorf, 1991.
- [5] N. Rebelo, J.C. Nagtegaal, L.M. Taylor and R. Passmann, Comparison of implicit and explicit finite element methods in the simulation of metal forming processes, in: J.L. Chenot, R.D. Wood and O.L. Zeinkiewicz (eds.), *Numerical Methods in Forming Processes*, Balkema, Rotterdam, 1992.
- [6] *ABAQUS/Standard: User's, Examples and Theory manuals*, Hibbitt, Karlsson & Sorensen, Inc., 1992.
- [7] *ABAQUS/Explicit: User's and Examples manuals*, Hibbitt, Karlsson & Sorensen, Inc., 1992.
- [8] A.P. Karafillis and M.C. Boyce, A general anisotropic yield criterion using bounds and a transformation weighting tensor, *J. Mech. Phys. Solid*, accepted.
- [9] J. Lian, F. Barlat and B. Baudelt, Plastic behavior and stretchability of sheet metals. Part II: Effect of yield surface shape on sheet forming limit, *Int. J. Plast.*, 5 131 (1989)
- [10] A.P. Karafillis and M.C. Boyce, On the modeling of contact in finite element analysis of forming processes, in: J.L. Chenot, R.D. Wood and O.L. Zeinkiewicz (eds.), *Numerical Methods in Industrial Forming Processes*, Balkema, Rotterdam, 1992.
- [11] J. Cao and M.C. Boyce, Draw bead penetration as a control element of material flow, *SAE Sheet Metal and Stamping Symposium, SP-944*, Detroit, 1993.